Journal of Constructional Steel Research 162 (2019) 105717

Contents lists available at ScienceDirect

Journal of Constructional Steel Research

journal homepage: www.elsevier.com/locate/ijcard

Full-scale test of a steel moment-resisting frame with composite floor under a penultimate edge column removal scenario

Junjie Wang [a, b], Wei Wang [a, b, *], Yihai Bao [c], Dawn Lehman [d]

[a] State Key Laboratory of Disaster Reduction in Civil Engineering, Tongji University, Shanghai 200092, China
[b] Department of Structural Engineering, Tongji University, Shanghai 200092, China
[c] Department of Civil and Environmental Engineering, University of California, Davis, CA 95616, United States
[d] Department of Civil and Environmental Engineering, University of Washington, Seattle, WA 98195, United States

ARTICLE INFO

Article history:
Received 18 April 2019
Received in revised form
30 July 2019
Accepted 31 July 2019
Available online 8 August 2019

Keywords:
Progressive collapse
Disproportionate collapse
Full-scale test
Composite floor
Steel moment connection

ABSTRACT

This study investigates the structural behavior and load-resisting mechanism of a typical composite floor system subjected to the penultimate edge column removal scenario. A 2 × 1 bay full-scale composite floor system is quasi-statically pushed down to failure under the displacement loading scheme. Full scale, moment-resisting connection, and continuous steel deck are three main features of this test. Based on this test, load-deflection responses, load-carrying mechanisms, deformation manners, and failure modes are discussed. The maximum load-carrying capacity was achieved at the flexural stage before the fracture of the girder-to-column connection, after that, the resistance decreased slightly and plateaued. The maximum static and dynamic load carrying capacities of the tested specimen is 4.2 times and 3.6 times of the ASCE load combination for accidental events, respectively. The damaged area of the composite floor is concentrated neighboring to the removed column, which is caused by the girder-to-column connection failure. Yield line method is used to predict the load-carrying capacity of this composite floor system, and the prediction agrees well with the maximum resistance measured in the test. After the failure of the girder-to-column connection in the removed column area, the measured loads are 15.9% ~ 24.5% higher than the predicted values. This is because the yield line method does not count the contribution of the tensile membrane action in the slab. By comparing with the results from previous experimental studies, the effectiveness of the moment-resisting connection and the continuous steel deck on improving the load-carrying capacity of the composite floor system has been validated.

1. Introduction

Progressive collapse of structures usually begins with the failure of a local structural component, and then successively spreads to the neighboring components, even leads to the collapse of the entire structure [1]. Design and strengthening methods to improve the progressive collapse performance of building structures can be found in the General Services Administration publication, GSA (2013) [2] and the Unified Facilities Criteria, DoD [3]. Alternative load path method, considering the column removal as the initial damage, is used in these two guidelines to design the structures to resist loads resulting from such damage. After the column removal, an alternative load path capable of resisting the load previously carried by the removed column is needed to be formed by the residual structural components.

Up to now, experimental researches focusing on the progressive collapse can be summarized into three different levels: (1) the subassemblage level; (2) one-story floor system level; and (3) full structural system level [4]. According to Hoffman and Fahnestock [5], for a building with an identical structural layout in each story, each story would only resist the gravity loads directly applied to itself, and the number of floors would not significantly change the response of a building under the progressive collapse. Therefore, considering the expenses and complexity, the one-story floor system testing may be the best choice.

Some researchers have conducted nonlinear finite-element analyses to investigate the progressive collapse behavior of the composite floor systems. Sadek et al. [6] computationally investigated the robustness of a gravity steel frame with the composite slab, whose results indicated that the steel deck could significantly improve the load-carrying capacity of composite floor systems. Alashker et al. [7,8] conducted a series of simulations to investigate the influence of key parameters, such as steel deck thickness, steel reinforcement ratio and shear-tab connection strength, on the robustness of composite floors subjected to the removal of a center column. It has shown that the main collapse resistance came from the steel deck and only three-dimensional models could accurately

* Corresponding author at: State Key Laboratory of Disaster Reduction in Civil Engineering, Tongji University, Shanghai 200092, China
E-mail address: weiwang@tongji.edu.cn (W. Wang).

https://doi.org/10.1016/j.jcsr.2019.105717
0143-974X/

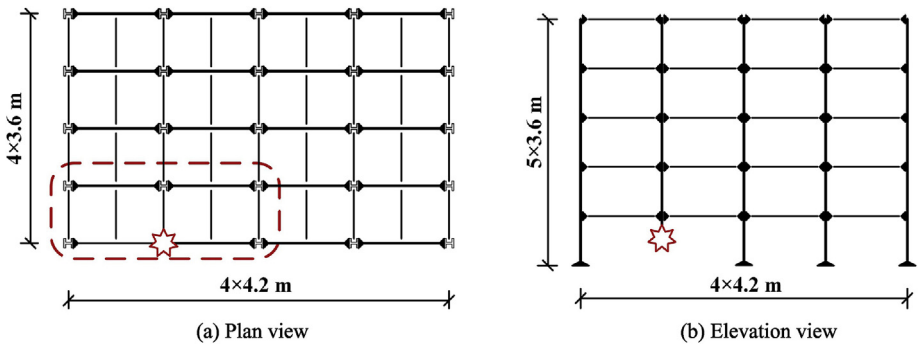

Fig. 1. Prototype structure.

reflect the complex collapse behavior of composite floor systems. Furthermore, an iterative design method was proposed based on the simulation results [9]. Li [10] compared different simplified approximations of structural models for progressive collapse analysis and found that the planar models tended to underestimate the structural robustness due to neglecting the slab contribution. Main and Liu [11] compared the behaviors of the gravity frame, the moment frame, and the braced frame. Both moment connections and steel braces could significantly enhance the load-carrying capacity of the floor system.

As the progressive collapse has been always accompanied by excessive nonlinearity and severe damage of structures, the numerical results need to be validated by high-quality experimental data. Recently, three outstanding experimental studies on floor systems have been conducted by Johnson et al. [12], Hadjioannou et al. [13], Fu et al. [14], respectively. Both Johnson et al. [12] and Hadjioannou et al. [13] tested a similar half-scale one-story composite floor system subjected to internal or edge column removals. The tested substructure was extracted from the gravity frame of a typical commercial building without any special enhancement for progressive collapse. However, the results of these two studies were quite different. All the test specimens conducted by Johnson et al. [12] could not sustain the design load combination, while the load-carrying capacities of the test specimens conducted by Hadjioannou et al. [13] were more than 1.7 times of the design load combination. Such a discrepancy may be caused by the stronger horizontal boundary restraints and the thicker slab used by Hadjioannou et al. [13] than that by Johnson et al. [12]. Fu et al. [14] investigated the collapse behavior of a one-third scale composite floor system with semi-rigid beam-column connections. The contribution of the composite slab and steel beams was quantified, where the composite slab could sustain at least one-third of the total vertical load.

All three experimental studies mentioned above were conducted on reduced scale specimens. As noted by Harris and Sabnis [15], in order to obtain accurate results, the reduced scale specimens must use the same materials as the prototype structures, and at the same time, all the geometric dimensions must be scaled with the same factor. As described by Johnson et al. [12], even if it was just a half-scale model, it was hard to find the desirable steel members to meet the geometrical scale factor at every location, especially for the profiled steel deck. Furthermore, the small-scale specimens usually adopt the plain round bar instead of the deformed bar in the prototype structure, where different bond behaviors are seen for these two types of bars. In general, the reduced scale specimen would be difficult to accurately and comprehensively reflect the actual behavior of the prototype structure. In this study, a full-scale specimen was designed and tested to overcome those shortcomings of reduced scale specimens.

As noted by Mitchell and Cook [16], the fully restrained interior panels could motivate the two-way tensile membrane action, whereas the edge panels may only develop the one-way tensile membrane action. In this sense, the edge column loss scenario would be more vulnerable than the interior column loss scenario. Therefore, the penultimate edge column removal scenario is adopted in this study. As suggested by Sadek et al. [6], Johnson et al. [12] and Hadjioannou et al. [13], moment-resisting connections and the continuity of steel deck could increase the load-carrying capacity under the column removal scenarios. The effectiveness of these recommendations will be validated in this study by testing a full-scale composite floor system under a penultimate edge column removal scenario.

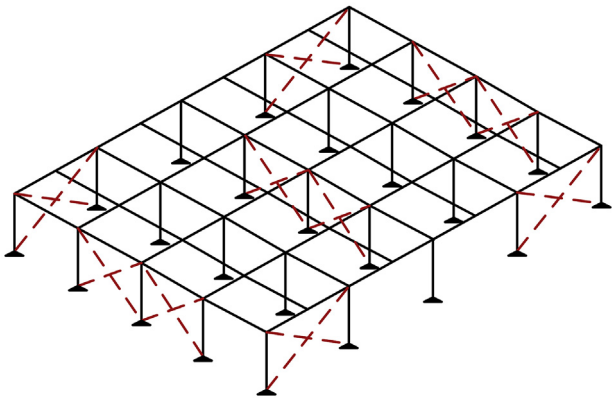

Fig. 2. Layout of steel bracing.

2. Experimental program

2.1. Prototype structure

To reflect the real structural behavior of composite floor systems, a prototype building with a typical structural configuration (Fig. 1) has been designed based on the Chinese codes [17,18]. This prototype building is a 4×4 bay five-story steel-concrete composite framed structure commonly used in East Asia. The story height is 3.6 m, and the span length of girders and beams are 4.2 m and 3.6 m, respectively. The design dead load (DL) and live load (LL) are 5 kN/m^2 and 2 kN/m^2, respectively. The design basic earthquake acceleration is 0.1 g, and the design basic wind pressure is 0.55 kN/m^2. Lateral loads are resisted by the steel bracing system as shown in Fig. 2.

Table 1
Geometrical dimensions of structural elements (dimension in mm).

Structural elements	$H \times B \times t_w \times t_f$
Girder	H200 × 100 × 5.5 × 8
Beam	H150 × 75 × 7 × 10
Column	H200 × 200 × 8 × 12
Brace	H100 × 100 × 6 × 8

Note: H, B, t_w and t_f represent the section height, section width, web thickness and flange thickness, respectively.

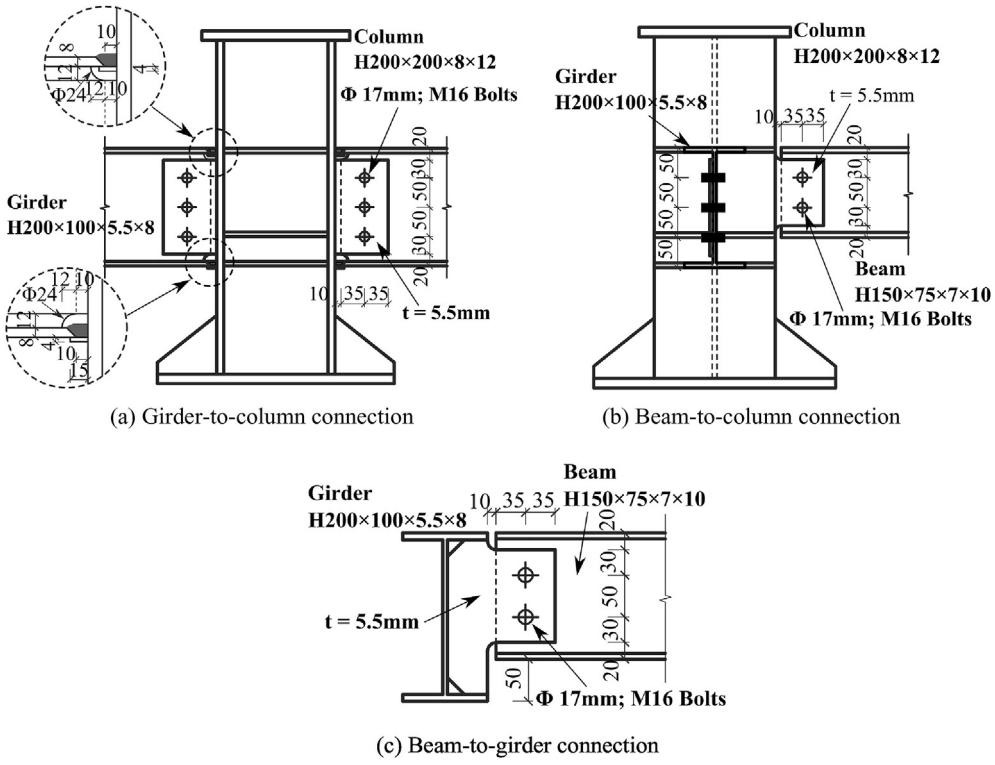

Fig. 3. Connection details of prototype structure.

All the girders, beams, columns and braces are made by hot-rolled H-section (with Q345 steel, which is equivalent to the ASTM A572 Grade 50 steel in the United States). The dimensions are listed in the Table 1. As shown in Fig. 3 (a), the girders are connected to the column through moment resisting connections with welded flanges and bolted web. Complete penetration groove welds are used to connect the girder flanges to the column flange, and three M16 (16 mm in nominal diameter) Grade 10.9 slip-critical high-strength bolts are employed to connect the girder web with the extended shear tab. As shown in Fig. 3 (b) and (c), the transverse beams are connected to the columns and girders with the extended single shear tab using two M16 Grade 10.9 slip-critical high-strength bolts. All the high-strength bolts are applied with a pre-tightening force of 100 kN.

As shown in Fig. 4, the composite floor has a 50 mm thick concrete slab above the 50 mm deep trapezoidal steel deck. The steel deck is LF2-915 with a thickness of 1.2 mm and a width of 915 mm. The laying direction of the trapezoidal steel deck is parallel to the girder direction. The C30 concrete slab is reinforced with 200 × 200 mm CRB550 welded steel fabric. The nominal compressive strength of the C30 concrete is 30 MPa. The concrete cover of the welded steel fabric is 15 mm. The girders and the beams are composite with the concrete slab by shear studs with 16 mm in diameter and 80 mm in height. To achieve the full composite action, a total of 13 shear studs are welded to each girder with a 300 mm spacing, while 11 shear studs are welded to each beam with a 305 mm spacing.

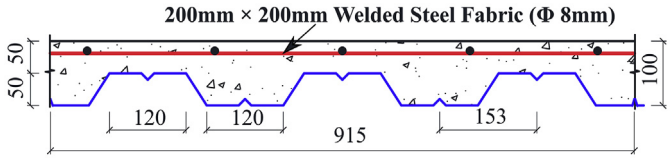

Fig. 4. Details of composite slab.

2.2. Test specimen

As shown in Fig. 1, a penultimate edge column located at the first floor is assumed to be removed. The directly affected exterior panel, named 2G1B-OUT, has been extracted from the prototype structure, as highlighted by the dashed line in Fig. 1 (a). The plan view and elevation view of 2G1B-OUT are shown in Fig. 5. The columns, girders, beams and peripheral beams are represented by “C,” “G,”

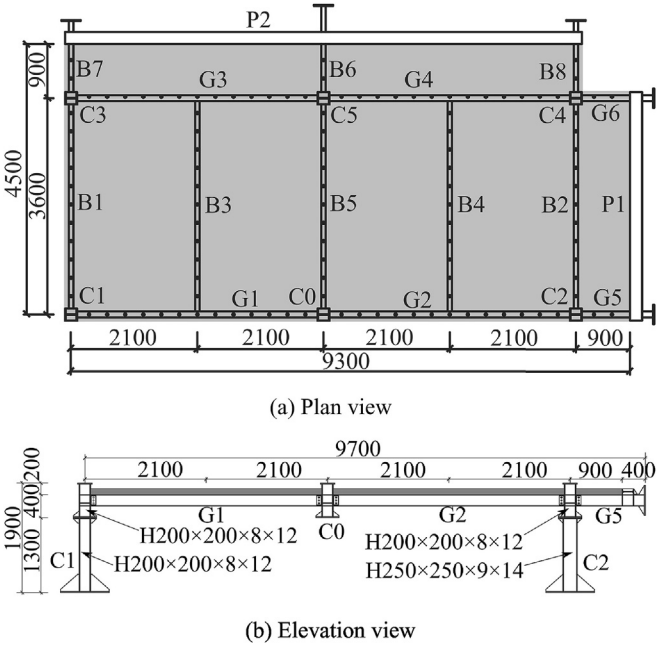

Fig. 5. Test specimen.

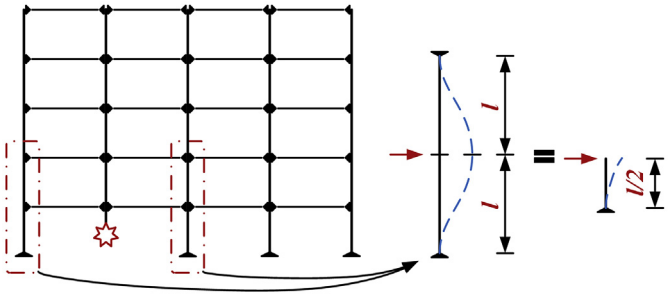

Fig. 6. Simplification of column.

"B" and "P," respectively. The extended 900 mm wide slab is designed to simulate the boundary conditions provided by the neighboring spans. The welded steel fabrics and steel deck in the extended slab have been welded to the peripheral beams, which have been constrained to the extended girders and extended beams as shown in Fig. 5. The peripheral beams have the same section size and material property as that of the girders. The trapezoidal steel deck is continuous without any overlapping along the girder direction and has a total length of 9400 mm. In the direction parallel to the beam, each piece of steel deck has a width of 915 mm, and the neighboring steel decks are interlocked by the deformed ribs. The welded steel fabric has a lap splice of 600 mm above the B5 and B6 beams to keep the reinforcement continuity.

Due to the limited laboratory space, a specimen with full-height columns would not fit. As shown in Fig. 6, assuming the bottoms of the first-floor columns and the tops of the second-floor columns are fixed, the lateral stiffness of the two adjacent columns can be calculated by Eq. (1).

$$k_{adjacent} = \frac{2 \times 12EI}{l^3} = \frac{24EI}{l^3} \tag{1}$$

Meantime, the lateral stiffness of a half-story height cantilever column with the same section size can be calculated by Eq. (2). Since the cantilever column has the same lateral stiffness as the two adjacent columns, it is used to replace the two adjacent columns in the specimen approximately.

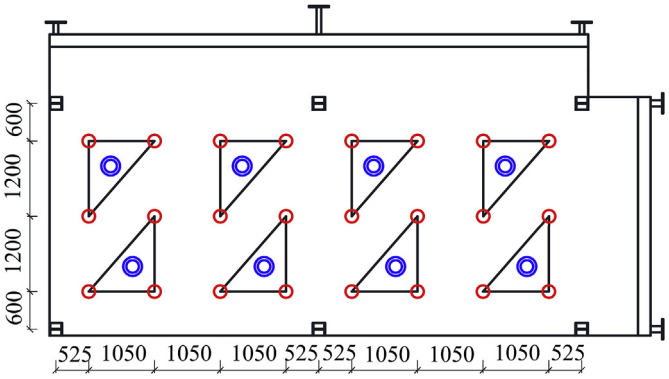

Fig. 8. Loading points of load-distribution system.

$$k_{cantilever} = \frac{3EI}{(0.5l)^3} = \frac{24EI}{l^3} = k_{adjacent} \tag{2}$$

As shown in Fig. 2, there are steel braces in the outside girder span of the 2G1B-OUT. The steel braces can significantly enhance the loading carrying capacity under the progressive collapse scenario as indicated by Main and Liu [11]. In this test, it is difficult to arrange the steel braces within the half-story height space. Therefore, the steel braces are not taken into account, leading to a relatively conservative result from this study. The specific effect of the steel braces will be investigated numerically in the future. For the convenience of transportation, all the columns are divided into two parts, as shown in Fig. 5(b), one 600 mm stub and one 1300 mm support column. During the component fabrication and concrete casting, the support column did not connect to the test specimen. As part of a series of experimental tests, the support columns of C2, C4, and C5 are replaced by the H250 × 250 × 9 × 14 (mm) hot-rolled steel (Fig. 5(b)), which can be reused for another specimen. Since the Column C2, C4, and C5 are constrained to the horizontal constraints, this change of the column section size has limited influence on the overall behavior of the floor system.

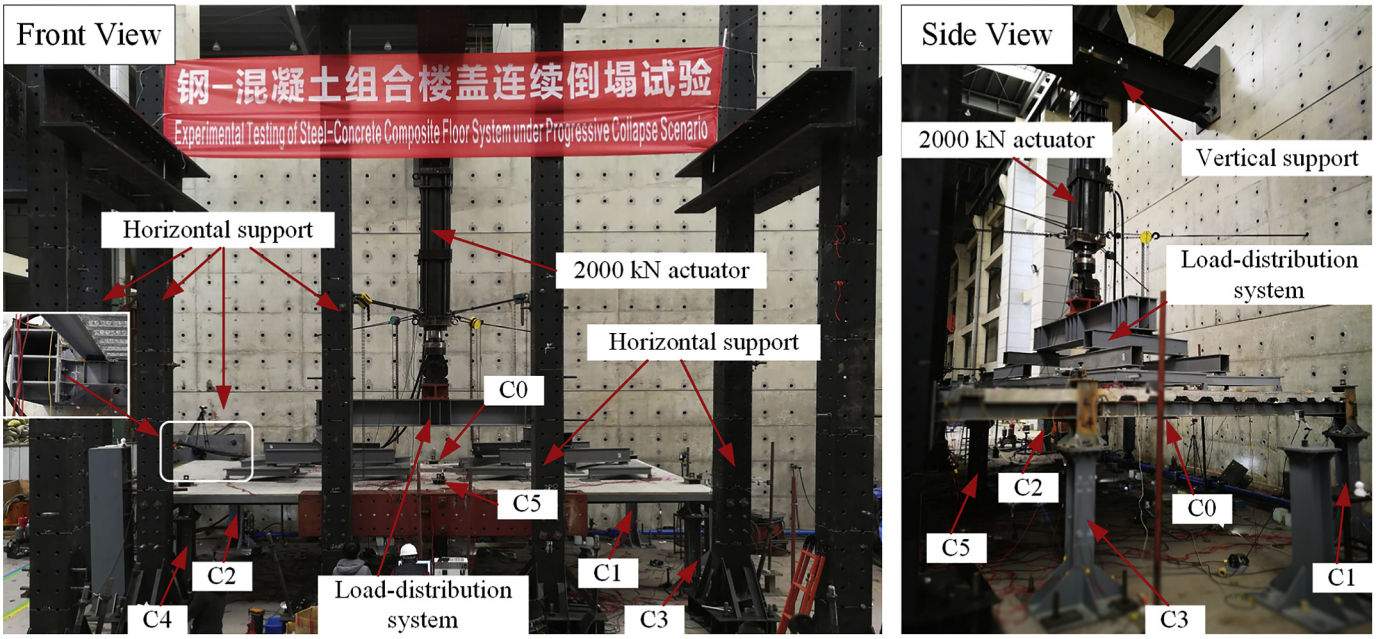

Fig. 7. Test setup and boundary conditions.

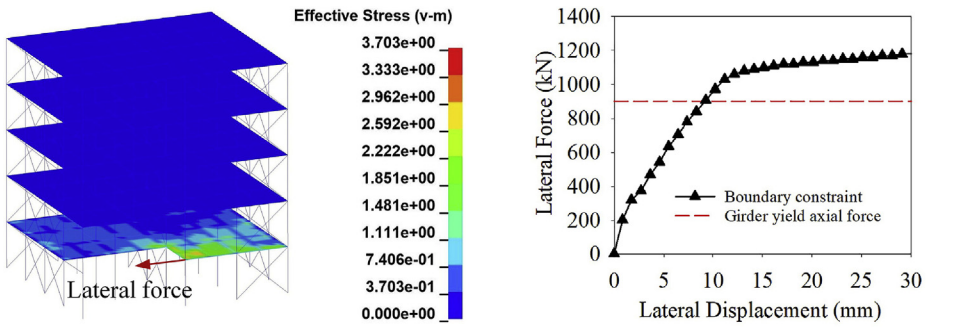

(a) Prototype structural model (b) Force-displacement curve of lateral constraint

Fig. 9. Lateral constraint of the test specimen.

2.3. Test setup and procedure

The test setup of 2G1B-OUT is shown in Fig. 7. The point load from the 2000 kN actuator is uniformly distributed to the 24 loading points by the load-distribution system (Fig. 8). There are four levels in the load-distribution system, including seven strong beams and eight triangular steel plates. The distribution beams except the third level beam are connected by steel rollers and loosely restricted with bolts in an oblong slot, which forms a pin connection between different level beams without losing stability. The third level beam is connected to the triangular steel plate by a socket joint, allowing the possible rotation when the slab is undergoing large deflection. The point load from the 2000 kN actuator is vertically mounted onto the mid-span of the first level distribution beam. The load of every triangular steel plate is distributed to three 300 × 300 mm square plates to avoid the punching shear failure. The actuator is loaded under the displacement-control loading scheme with a 4 mm/min loading rate.

As illustrated in Fig. 7, the extended girders, i.e., G5, G6, and extended beams, i.e., B6, B7, B8, are fully constrained to the horizontal supports to simulate the boundary condition provided by neighboring structural components. The horizontal support connected to G5 is the most important one in this test because its horizontal stiffness will significantly influence the catenary force developed in G2. The fully constrained assumption of this support is validated by comparing with the horizontal reaction in the prototype structure. As shown in Fig. 9 (a), a structure model representing the residual structure after removing the test specimen is established in LS-DYNA. Beam elements with cross-section integration are used to model the column, girder, beam, and brace, while the composite slab is modeled with shell elements with cross-section integration. Nominal values are adopted for the material properties in this preliminary model, i.e., 345 MPa for structural steel components and steel deck, 550 MPa for welded steel fabrics and 30 MPa for concrete. A lateral force is applied to the joint on behalf of the G5-C2 connection in the test specimen, and the corresponding force-displacement curve is plotted in Fig. 9 (b) along with the yield axial force (901 kN) of the G5 girder. It is shown that an insignificant horizontal displacement (9 mm) occurs when the laterally applied force reaches the yield axial force of G5, therefore the fully constrained assumption of the horizontal support connected to G5 is considered to be reasonable.

2.4. Instrumentation

The test specimen is monitored with a set of instruments to capture both global and local behaviors. A total of 27 LVDTs (linear variable differential transducer) are used in this specimen. Twenty-one LVDTs (marked by V) is used to capture the vertical deflection patterns of the floor system, and 6 LVDTs (marked by H) are used to measure any possible horizontal movement in the peripheral components. Besides, the strains of the columns, girders, beams, trapezoidal steel decks and welded steel fabrics are measured by a number of uniaxial strain gauges. These measured strains are used to analyze the stress and load redistributions of the specimen. The instrumentation arrangement will be introduced in the later sections.

2.5. Material properties

Coupon tests have been carried out to obtain the actual steel properties. The steel properties of the columns, girders, beams, trapezoidal steel decks and welded steel fabrics are listed in Table 2. The values of elongation are calculated based on the reference length and rupture length. Since no coupon test has been conducted for the shear studs and high-strength bolts, the nominal material properties provided by the manufacturers are adopted and listed in Table 2.

Table 2
Material properties from coupon tests (dimension in mm).

Location		Initial Thickness	f_y (MPa)	f_u (MPa)	Reference length	Rupture length	Elongation[a]
Girder/Peripheral beam	Flange	7.7	390	536	80	105	0.31
	Web	5.3	419	557	70	92	0.31
Beam	Flange	9.3	365	517	90	118	0.31
	Web	6.5	400	535	75	99	0.32
Column	Flange	11.6	373	531	100	132	0.32
H200 × 200	Web	7.8	395	546	80	105	0.31
Column	Flange	13.4	383	536	110	142	0.29
H250 × 250	Web	8.6	405	551	85	107	0.26
Steel deck	Slab	1.18	320	380	60	83	0.38
Rebar	Slab	Φ 8	596	672	50	53.3	0.07
Shear stud	Slab	Φ 16	320	400			0.14
Bolt	Connection	Φ 16	940	1040			0.10

[a] Elongation = (Rupture length)/(Reference length)-1.

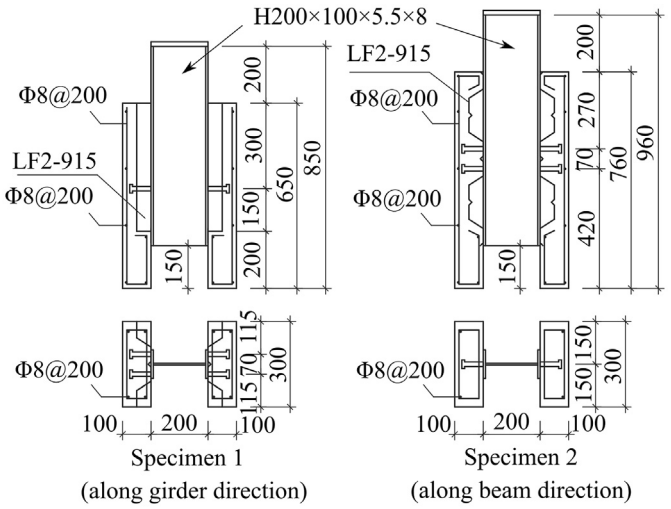

Fig. 10. Push-out specimens.

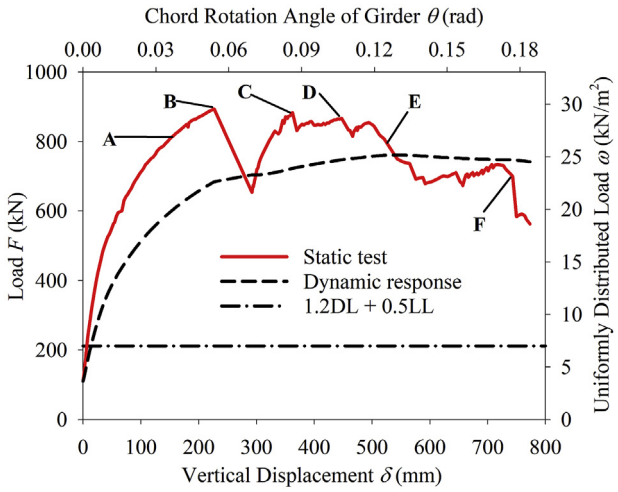

Fig. 12. Load-displacement curve of 2G1B-OUT.

The concrete compressive strength is measured with 150 mm × 150 mm × 150 mm cube samples, and the average value is 32.83 MPa. Two shear stud push-out tests have been conducted to study the composite behavior and provide test data for future numerical validations. As shown in Fig. 10, Specimen 1 represents the shear studs along the girder direction, and Specimen 2 represents the shear studs along the beam direction. The materials used in the push-out specimens are identical to those of Specimen 2G1B-OUT. Displacements are measured by the built-in transducer in the actuator. The relative load-displacement curves are plotted in Fig. 11, which shows a better performance of Specimen 1 comparing to Specimen 2 regarding capacity (around two times higher) and ductility.

3. Experimental responses

3.1. Failure process and load-carrying capacity

The load-displacement curve is shown in Fig. 12. The load F was measured from the actuator, while the displacement δ was calculated by the average value of the measured displacements from two LVDTs attached to the bottom of the C0 column. The uniformly distributed load ω was obtained by dividing *F* by the area of the 2 × 1 bay floor (8.4 m × 3.6 m = 30.24 m^2), and the chord rotation angle of girder θ was calculated by dividing δ by the girder span (4.2 m). Considering the self-weight of the 2 × 1 bay floor (66.4 kN) and the weight of the load-distribution system (44 kN), there is an equivalent initial distributed load of 3.65kN/m^2 before loading. The failure process of Specimen 2G1B-OUT will be described according to the load-displacement curve as follows.

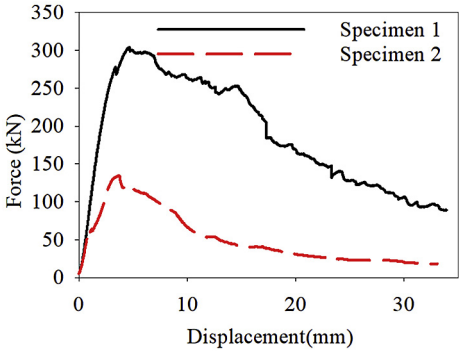

Fig. 11. Load-displacement curves of push-out specimens.

When the vertical displacement reached 156 mm (0.037 rad, 815.9 kN, Point A), concrete cracks were observed above the B3-G1 connection (Fig. 13(a)), which were caused by the excessive shear force transferring from the B3 beam. While the vertical displacement reached 226 mm (0.054 rad, 893.5kN, Point B), the applied load suddenly dropped from 893.5 kN to 608 kN due to the bottom flange fracture at the G2-C0 connection followed by the upper flange fracture (Fig. 13(b)). The maximum resistance of 893.5 kN was achieved at Point B, where the first peak load during the entire loading process was observed. In the meantime, concrete cracks developed around the C0 column due to the excessive compression (Fig. 13(b)). The slab above the B4-G2 connection also cracked similar to the slab above the B3-G1 connection (Fig. 13(a)). After the sudden load drop, the resistance quickly bounced back. When the vertical displacement reached 363 mm (0.086 rad, 885 kN, Point C), the resistance achieved a second peak load of 885 kN. After that, the load dropped slightly to 831 kN due to the upper flange fracture of the G2-C2 connection (Fig. 13(c)). As the vertical displacement reached 432 mm (0.103 rad, 859.7 kN, Point D), the upper flanges of G1-C1 connection and G2-C0 connection fractured (Fig. 13(d) and (e), respectively). The G2 girder was connected to the C0 column by the shear tabs only. Severe cracks were observed along the C3-C5-C4-C2 direction, i.e., the hogging moment region. Severe cracks also formed along the C0-C5 direction, resulted from the G2-C0 connection fracture. When the vertical displacement reached 550 mm (0.131 rad, 744.0 kN, Point E), the G2-C0 connection completely failed (Fig. 13(f)), and the applied load decreased to about 680 kN. The complete failure of the G2-C0 connection indicated both the flexural action and the catenary action provided by the girders were diminished to zero. The applied load was mainly born by the slab. Due to the failure of G2-C0 connection, the concrete spalled around the C0 column, and the rebars were exposed to the outside. When the vertical displacement further increased to 741 mm (0.176 rad, 721.6kN, Point F), the applied load dropped from 721.6 kN to 581 kN. The steel deck near the C0 column fractured (Fig. 13(g)) due to the excessive tensile membrane force developed in the slab. The slab adjacent to the C0 column was seriously damaged. The connection between the slab and the B5 beam failed as the shear studs were pulled out from the slab (Fig. 13(g)). The steel deck and the rebars also fractured at the area adjacent to the C2 column (Fig. 13(h)). The test was then terminated due to the excessive damage. The final state of 2G1B-OUT is shown in Fig. 14.

From the load-displacement curve, the applied vertical load achieved its maximum peak load of 893.5kN at the vertical displacement of 226 mm under the flexural stage. After the sudden

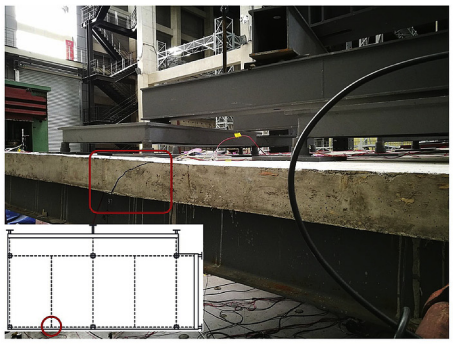

(a) Concrete cracks above the B3-G1 connection

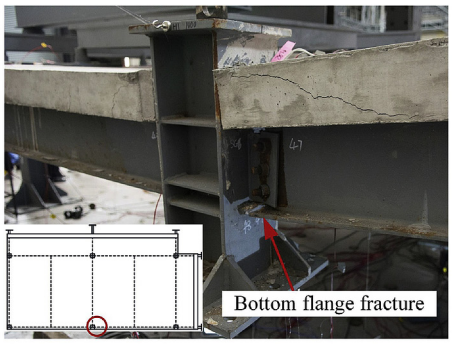

(b) Failures around C0 column

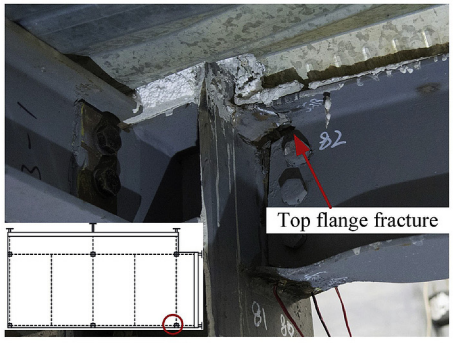

(c) Top flange fracture at the G2-C2 connection

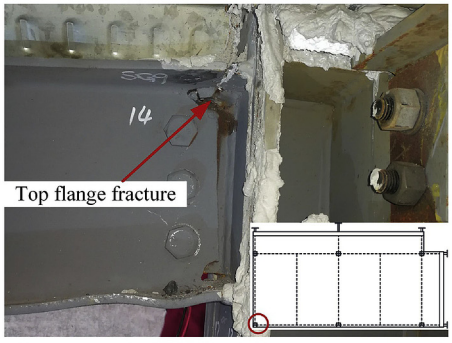

(d) Top flange fracture at the G1-C1 connection

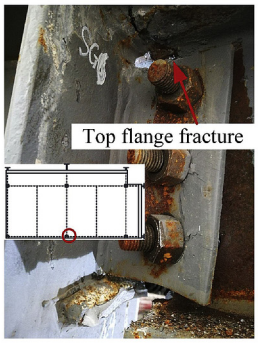

(e) Top flange fracture at the G2-C0 connection

(f) Totally failure of the G2-C0 connection

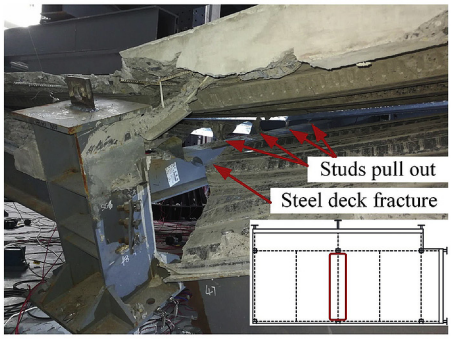

(g) Fracture of the steel deck near C0 column

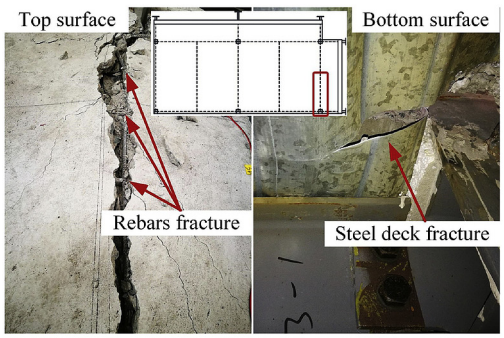

(h) Steel deck fracture adjacent to C2 column

Fig. 13. Failure phenomenon in the loading process.

load drop due to the flange fracture at the G2-C0 connection, the applied load increased to a steady platform of about 850kN, which can be seen as the transitional stage between the flexural stage and the catenary and membrane stage. The complete failure of the G2-C0 connection at the vertical displacement of 550 mm indicated the vanishing of the girder catenary action. The applied load was carried by the residual low flexural resistance and mostly the tensile membrane action of the slab. The floor system can sustain a vertical load of 732 kN, however, this load does not surpass the peak load in the flexural stage.

Fig. 14. Failure phenomenon at the end of the test.

According to the ASCE 7-16 [19], the load combination for accidental events is 1.2 DL + 0.5 LL. As to this specimen, the load combination value is 7 kN (1.2 × 5 kN + 0.5 × 2 kN). The peak load that can be sustained statically by the specimen is 29.5 kN/m^2. The load-carrying capacity of the tested specimen is about 4.2 times of the ASCE load combination. Using the energy method proposed by Izzuddin [20], the corresponding dynamic response can be derived and is plotted in Fig. 12. The maximum dynamic resistance 761 kN (or 25.1kN/m^2) is 3.6 times of the ASCE load combination. In conclusion, this steel-concrete composite floor system with 4.2 m girder span and 3.6 m beam span designed according to Chinese design specifications could withstand the penultimate edge column removal.

3.2. Displacement contour

The arrangement of the LVDTs is shown in Fig. 15. The vertical slab deflection contour at the displacement of 650 mm is plotted in Fig. 16. Larger vertical displacement is observed in the slab area between B1 and B5 (Fig. 16). The center point of this area (V16) has almost the same displacement as that of the C0 column. This observation indicates a yield line generated in the slab along the C0-C3 direction. The vertical deflection of G1-C0-G2 almost developed symmetrically until the complete failure of the G2-C0 connection, leading to a sudden increase of the displacement of the G2 girder.

The horizontal movements of the specimen boundaries are plotted in Fig. 17. The horizontal movements of the column were measured at the top of the column stub, while the horizontal movements of the beam were measured at the mid-point of the beam cross-section. The movements toward the center of the specimen are defined as positive, and movements away from the center of the specimen are defined as negative. The horizontal

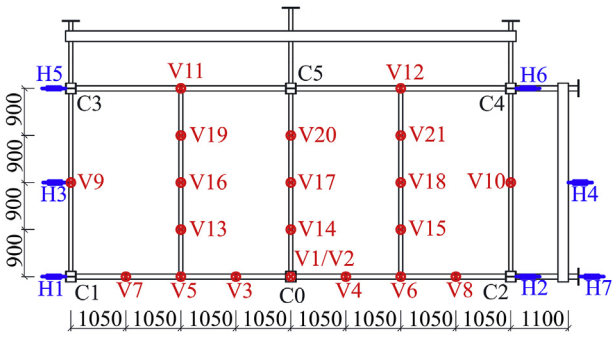

Fig. 15. Locations of the LVDTs.

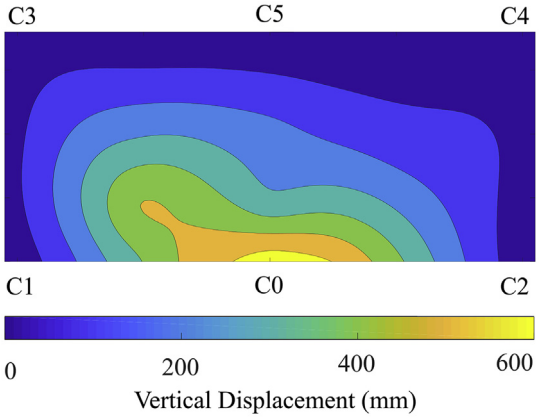

Fig. 16. Vertical deflection of the floor system at the displacement of 650 mm.

movements near C1 and C2 columns were similar when the vertical displacement was less than 450 mm. When the vertical displacement was beyond 450 mm, the movement near the C1 column was significantly greater than that near the C2 column. Since the horizontal movement at the horizontal support connected to G5 (H7) was almost zero, the horizontal movement at the C2 column implied that G5 was under compression. While the horizontal displacements at the C1 and C2 columns are outward, the displacements at the C3 and C4 columns are inward. This difference may arise from the G2-C0 connection failure and the steel deck fracture along the B5 beam, forming a trend to tear the specimen along the B5 beam. Similar to the case of C1 and C2 columns, the horizontal displacement at the C3 column was much greater than that at the C4 column. No horizontal movement was observed at the midspan of the B1 and P1 beams.

3.3. Slab crack pattern

The crack pattern of the slab's top surface at the final stage is shown in Fig. 18. Severe concrete crushing was seen at the area near the C0 column, and the cracks developed along C3-C0, C5-C0 and C4-C0 directions. No obvious concrete crushing was observed at the area near the C1 and C2 columns. A similar crack pattern has been also observed by Dat and Tan [21] during a concrete slab testing under the penultimate edge column removal scenario. The yield lines of this specimen are illustrated in Fig. 18, in which solid red lines represent the yield lines at the sagging moment region and dashed red lines represent the yield lines at the hogging moment

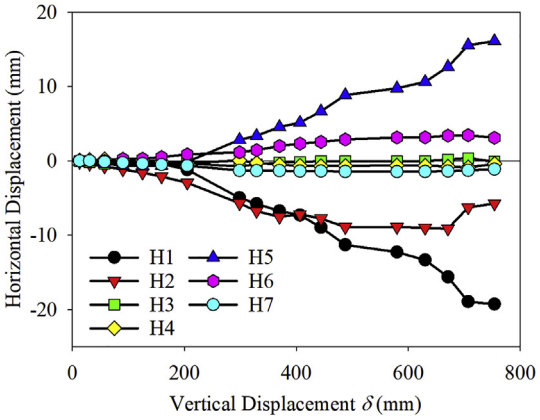

Fig. 17. Horizontal displacement of boundaries.

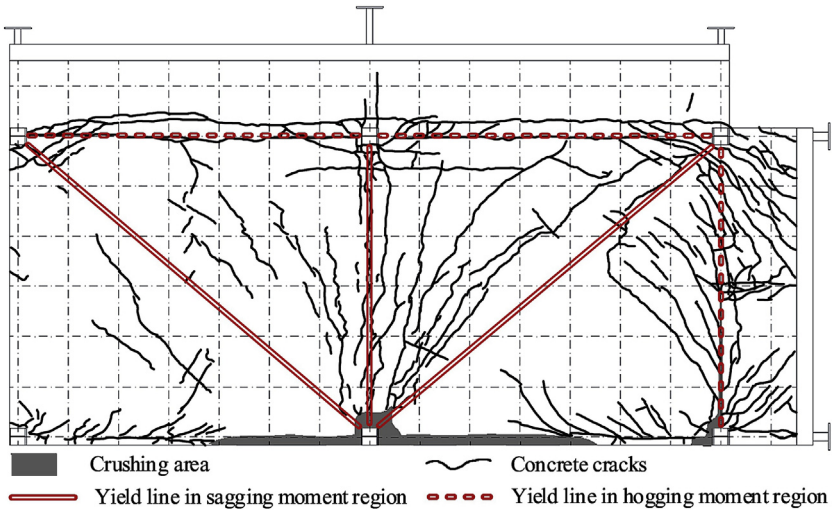

Fig. 18. Crack patterns at the slab top surface.

region. The result shows all yield lines in the panel area are directly linked to the removed edge column C0. This failure pattern is related to the girder-to-column connection failure near C0. The moment and axial force originally resisted by this girder-to-column connection were redistributed to the neighboring slab, which led to the tearing of the steel deck in Fig. 13(g) at the final stage. It is thus recommended that increasing the rotational capacity of the perimeter girder-to-column connection would effectively enhance the progressive resistance of the composite floor system. More details will be discussed later in Section 4.4.

4. Discussion of experimental results

4.1. Horizontal boundary force

The girder's catenary action is heavily dependent on the horizontal tensile forces developed at the girder ends. Consequently, the development of the horizontal boundary forces could reflect the development of the catenary action in the girders. As shown in Fig. 19, the moments of the support column at heights of H1 (1000mm) and H2 (500mm), i.e., M1 and M2, are calculated based on strain measurements recorded by the strain gauges attached to these sections. The shear force V in the column can be statically determined through Eq. (3). The axial force $F_{boundary}$ in the extended girder or beam can be derived by the measured strains at the girder or beam section. For the C2 and C4 columns, the horizontal force $F_{tension}$, representing the resultant of all horizontal forces at the girder-column connection, can be obtained by Eq. (4). For the C1 and C3 columns, the horizontal force $F_{tension}$ is equal to the shear force V (Eq. (5)). The positive value of $F_{tension}$ indicates that the tensile force has developed, and this tensile force can pull the corresponding column inward. The negative value of $F_{tension}$ indicates the corresponding column moving outward.

$$V = \frac{M_2 - M_1}{H_1 - H_2} \tag{3}$$

$$C2\ (C4) : F_{tension} = F_{boundary} + V \tag{4}$$

$$C1\ (C3) : F_{tension} = V \tag{5}$$

As shown in Fig. 20, the horizontal forces at C1 and C2 columns were compressive before the vertical displacement reached 410 mm, and then gradually turned into tension as the vertical displacement increasing. Although the two horizontal forces have a similar development trend, the compression at the C2 column was greater than that at the C1 column as the vertical displacement was relatively small due to the horizontal constraint. At the final stage, the tension forces at C1 and C2 columns were caused by the torsional moment transferred from the neighboring beam. With the increasing of the vertical displacement at the loading slab area, B1 and B2 beams rotated around their axes. Then, these torsional moments were transferred to C1 and C2 columns causing the equivalent tensions in these areas. For C3 and C4 columns, the torsional moment transferred from B1 and B2 beams is counterbalanced by the extended beams (B7 and B8) and girders (G3 and

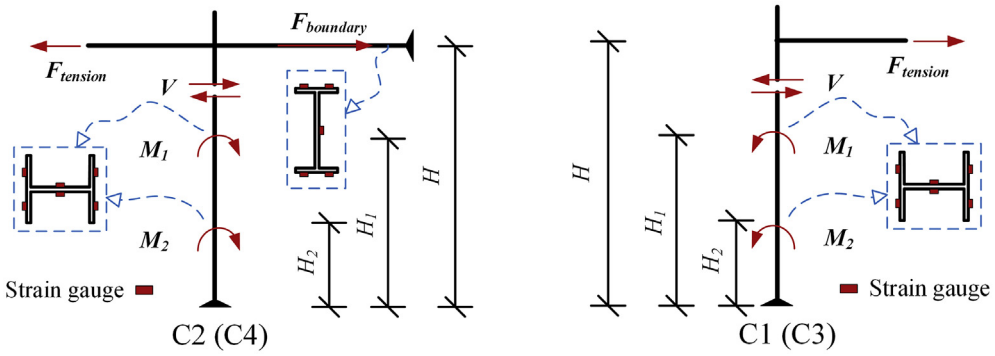

Fig. 19. Horizontal forces at the boundary columns.

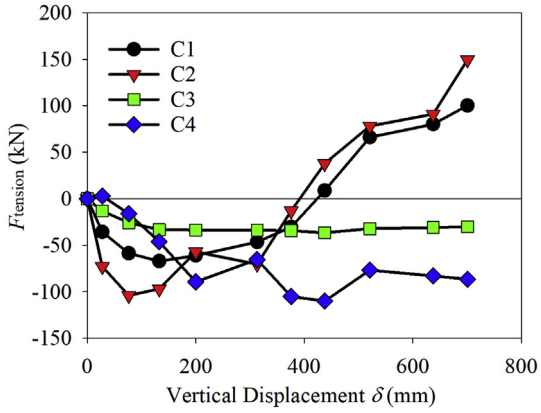

Fig. 20. Development of the horizontal force at each boundary column.

G4), therefore, both horizontal forces are compressive during the entire testing process.

4.2. Load redistribution of the columns

When a column in a building is suddenly removed, the load resisted by the lost column will be redistributed to the neighboring columns. The load redistribution ratios in these columns could reflect the alternative load paths formed in this floor area. The load redistribution ratios in the columns at four typical vertical displacements are illustrated in Fig. 21. These load redistribution ratios are calculated by dividing the vertical load by the axial force of each column, which is calculated based on the strain gauge measurements. The vertical load carried by the C2 column was always higher than that of the C1 column. The load ratio of the C2 column decreased after the fracture of the bottom flange at the G2-C0 connection, indicating the damage at the girder-to-column connection could weaken the load transfer through the G2 girder. Except for the temporary increase at a vertical displacement of 300 mm, the load ratio of the C5 column kept decreasing, indicating the load transfer capacity of the cantilever beam B5 decreased. The neighboring C3 and C4 columns carried the decreased load portion from the C5 column. As the loads transferred to the C1 and C5 columns were limited, the load ratio of the C3 column kept increasing during the testing process.

4.3. Yield line prediction of load-carrying capacity

As noted in Section 3.3, several yield lines were explicitly formed in the concrete slab. Therefore, the yield-line method was used to predict the load carried by the flexural mechanism. Based on the concrete crack pattern in Fig. 18, the yield-line configuration of the specimen is described in Fig. 22. $l_x = 8400\,mm$ and $l_y = 3600\,mm$ are the total length of the slab in the x- and y-directions. $\theta_x = 2\delta/l_x$ and $\theta_y = 2\delta/l_y$ are the rotation of the plastic hinges about the y-axis and x-axis, respectively, where δ is the vertical displacement at the C0 column. M_g and M'_g are the ultimate positive and negative bending moments of the girder, while M_b and M'_b are the ultimate positive and negative bending moments of the beam. The contribution of the composite slab to the bending moments of girder and beam has been considered. m_{sx} and m_{sy} are the ultimate positive bending moments of the per unit width composite slab in the x- and y-directions, while m'_{sx} and m'_{sy} are the ultimate negative bending moments of the per unit width composite slab in the x- and y-directions. All the ultimate bending moments are determined according to Johnson et al. [22], with the corresponding results listed in Table 3.

The internal virtual work $W_{internal}$ produced by positive and negative bending moment at the beam plastic hinges and slab yield lines is calculated in Eq. (6).

$$W_{internal} = \left(m'_{sx}l_y + 2m_{sx}l_y + 2M_g + 2M'_g\right)\theta_x + \left(m'_{sy}l_x + m_{sy}l_x + 2M_b + 2M'_b\right)\theta_y \quad (6)$$

The external virtual work $W_{external}$ done by the downward uniform distributed load ω on the slab is

$$W_{external} = \omega l_x l_y \delta/3 \quad (7)$$

ω can be derived by $W_{internal} = W_{external}$

$$\omega = \frac{3}{l_x l_y}\left[\frac{2\left(m'_{sx}l_y + 2m_{sx}l_y + 2M_g + 2M'_g\right)}{l_x} + \frac{\left(m'_{sy}l_x + m_{sy}l_x + 2M_b + 2M'_b\right)}{l_y}\right] \quad (8)$$

Based on the bending moment in Table 3, the yield-line prediction of ω is 27.8 kN/m^2 and the equivalent resultant force ($F = \omega l_x l_y$) is 840.8 kN. The measured maximum vertical resistance of the specimen is 893.5 kN ($\delta = 226$ mm), which is only 6.3% higher than the yield line prediction. As shown in Fig. 12, the vertical resistances between Point C (the ascending peak after the girder flange fracture) and Point E (the resistance drop caused by the girder connection failure) are very close to the yield-line prediction, demonstrating that the load-carrying capacity in this stage is mainly provided by the flexural mechanism.

As shown in Fig. 12, the load increased from 680 kN to 730 kN between the local minimum load near point E and the local peak load near point F. At this stage, the experimentally measured load is about 15.9% ~ 24.5% higher than the yield line prediction (586.5 kN). The portion of the vertical resistance exceeding the resistance predicted by the yield-line theory is mainly attributed to the tensile membrane action since the girder catenary action cannot be developed due to the G2-C0 connection failure. The fracture of the steel deck and steel fabrics (Fig. 13 (g)) near the C0 column also confirmed the development of this tensile membrane action.

4.4. Comparison with previous floor tests

The test results in this study have been compared with the previous composite floor tests conducted by Johnson et al. [12], Hadjioannou et al. [13], and Fu et al. [23], as listed in Table 4. Both the specimens tested by Johnson et al. [12] and by Hadjioannou

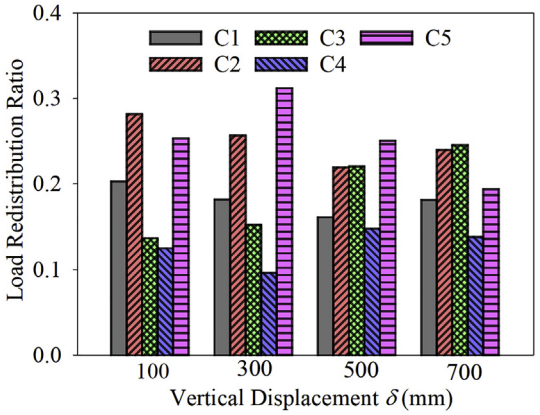

Fig. 21. Load redistribution ratio of every column.

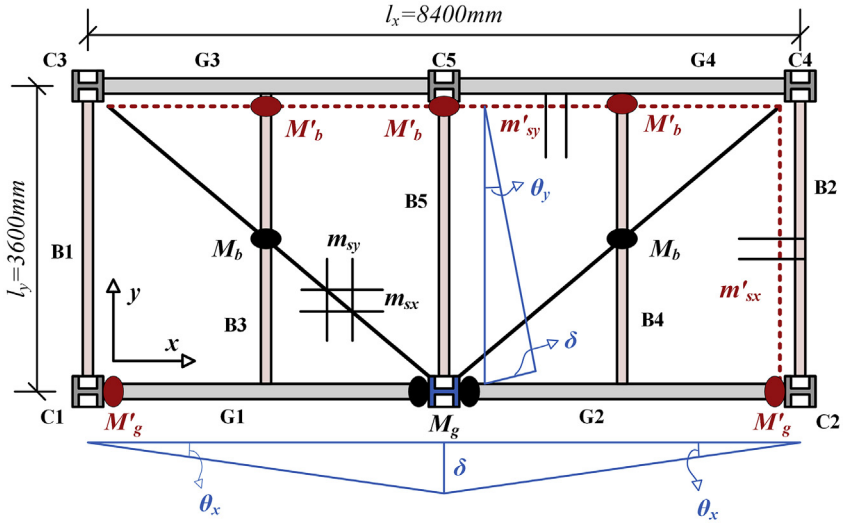

Fig. 22. Yield-line configuration of the test specimen.

et al. [13] used simple connection to connect the girder or beam to the column, while the girder-to-column connection chosen by Fu et al. [23] was semi-rigid connection. The girder spans in these tests were 4.5 m [12,13], 2 m [23] and 4.2 m (this study). Another difference between these tests was the loading methods: water load was used in Johnson et al. [12] and Hadjioannou et al. [13] by pumping water into the water tanks on the slab; load-distribution system was used in this study and Fu et al. [23]. The main advantages of the load-distribution system were easy to control and could obtain the post-peak response of the floor system. Both Johnson et al. [12] and Hadjioannou et al. [13] considered the edge column removal scenario and inner column removal scenario, while Fu et al. [23] only considered the inner column removal scenario. However, the capacity of inner column removal scenario in Johnson et al. [12] was heavily affected by the previously tested edge column removal scenario, as the slab continuity at the shared edges with the previously loaded bays had been destroyed. On the contrary, the capacity of the inner column removal scenario in Hadjioannou et al. [13] was extremely high and exceeded the loading capacity of the test set-up. Eventually, collapse initiated after removing all the bolts connected to the removed column. Hence, the load-carrying capacity of the inner column removal scenario had not been successfully obtained in Johnson et al. [12] and Hadjioannou et al. [13], and will not be compared in this section. All the edge column removal scenarios tested in Johnson et al. [12] removed the penultimate column, which was similar to 2G1B-OUT. However, the removed edge column in Hadjioannou et al. [13] was the middle edge column, at the same time, the slab and girders were restrained to the relatively strong perimeter beams, which could reflect the actual lateral constraints from the surrounding bays. Four specimens under the inner column removal scenario were tested in Fu et al. [23], which considered different aspect ratio, column removal location and composite action. In the tests conducted by Fu et al. [23], at least three edges restrained the lateral movements at the girder or beam ends by the reaction frames, while the continuous boundary of the slab was simulated by extending the slab by 1/4 of their neighboring spans. Therefore, the boundary constraints in Hadjioannou et al. [13] and Fu et al. [23] were much stronger than those in Johnson et al. [12] and this study.

Table 3
Ultimate bending moments of beams and slabs.

Components	Bending moment (kN.m)	Components	Bending moment (kN.m/m)
M_g	178.0	m_{sx}	31.3
M'_g	78.1	m'_{sx}	11.3
M_b	124.5	m_{sy}	3.7
M'_b	17.9	m'_{sy}	3.1

In addition, the steel deck used in Fu et al. [23] was re-entrant steel deck, while the trapezoidal steel deck was chosen in other tests. As the width of each piece steel deck was finite, the steel decks in these tests were discontinuous in their transverse direction, and the neighboring steel decks were connected by locking the performed edges. Consequently, the tensile membrane force could only develop in the longitudinal direction of the steel deck, which was parallel to the deck ribs. In Johnson et al. [12] and Hadjioannou et al. [13], the steel decks were also discontinuous in the longitudinal direction, and they were connected by shear studs welded through the overlapped steel decks. However, the composite slab tests conducted by Francisco and Liu [24] showed that the shear stud connection was unable to develop enough tensile membrane force. Two primary reasons caused this issue: (1) the shear stud connections could not undergo large deformation and might fail too early to develop the tensile membrane action; (2) the longitudinal strength transferred by the shear stud connection was significantly smaller than the full capacity of the steel deck section. In this study and Fu et al. [23], the steel decks were continuous in the longitudinal direction, which would be benefit for the development of the tensile membrane action. Besides, steel deck tearing around the removed column also implied excessive tensile membrane force developed in this region. Whereas, the deck fracture caused by the membrane force was not observed in Johnson et al. [12] and Hadjioannou et al. [13], because the steel decks were pulled apart at the seams during the test. Furthermore, as noted by Alashker et al. [8], the steel deck thickness could significantly affect the floor's capacity under the column removal scenario. The steel deck thicknesses in these tests were 0.75 mm [12,13], 0.9 mm [23] and 1.2 mm (this study).

The critical chord rotation angles, at when the critical connection component failure (such as girder flange fracture or bolt failure) occurs, are related to the corresponding span-to-depth ratio, as shown in Fig. 23. According to the results in these tests, when the critical chord rotation angles reached, the resistance of the floor system would be equal or approximate to its peak load. As the progressive collapse of the floor system is a dynamic process, any critical connection component failure would cause a sudden load redistribution and induce a successive failure. As noted by Lee et al. [25], for the steel moment frames, the load-to-rotation responses

Table 4
Comparison of different composite floor test results.

Source	Specimen	Connection type	Span length (m)	Column loss scenario	Number of restrained edges	Steel deck	Span-to-depth ratio	Critical chord rotation angle (rad)	Load-carrying capacity (kN/m^2)	Compare with 1.2DL + 0.5LL
Present study	2G1B-OUT	welded flange - bolted web	4.2 × 3.6	Edge column	2	Trapezoidal	14	0.054	29.5	4.2
Johnson et al. [12]	EC-G	Double angle	4.5 × 4.5	Edge column	2	Trapezoidal	16.1	0.036	4.0	0.6
	EC-B	Extended shear tab			2		19.8	0.028	4.0	0.6
Hadjioannou et al. [13]	ECL	Double angle	4.56 × 4.56	Edge column	3	Trapezoidal	17.3	0.075	9.1	1.7
Fu et al. [23]	2 × 3-S-PI	Flush end plate	2 × 3	Inner column	3	*Re*-entrant	7.4	0.080	53.1	8.1
	2 × 3-S-IC		2 × 3		4		7.6	0.070	51.2	15.3
	2 × 3-W-IC		2 × 3		4		7.6	0.083	51.8	8.2
	2 × 2-S-IC		2 × 2		4		7.6	0.097	96.3	8.4

under a column removal scenario were similar if the span-to-depth ratio was similar. As the geometric dimensions were different in these tests, the span-to-depth ratio is used as a normalized parameter to compare them. Therefore, these tests are discussed based on the critical chord rotation angle and span-to-depth ratio. Both the critical chord rotation angles in the tests conducted by Fu et al. [23] and by Hadjioannou et al. [13] exceed 0.07 rad. However, the critical chord rotation angles in the tests conducted by Johnson et al. [12] did not exceed 0.036 rad, although a similar span length and connection type were used as the test in Hadjioannou et al. [13]. Moreover, the dominant connection failure mechanism in Johnson et al. [12] was bolt shear, while this phenomenon was not observed in Hadjioannou et al. [13]. This was primarily due to smaller bolt size (9.5 mm in diameter) used, since the bolt size used by Hadjioannou et al. [13] was 12.7 mm in diameter, which shear capacity was relatively higher. As the tests in Johnson et al. [12] were not horizontally constrained at the boundary, the floor load would be mainly resisted by the flexural mechanism. With bolt connection under tension and composite slab under compression, positive moment was developed at the removed column location. But, the bolt shear strength in Johnson et al. [12] was too weak to ensure this positive moment to achieve a larger rotation angle. The bolt size used in the present test and in the Fu's test [23] was 16 mm in diameter. Besides, the slab strength and the horizontal restraints of the floor system conducted by Hadjioannou et al. [13] were much stronger than that conducted by Johnson et al. [12]. Without considering the tests conducted by Johnson et al. [12], which used a relatively small bolt, the critical chord rotation angle of the rigid connection in the present study was 0.054 rad, smaller than those of the simple connection by Hadjioannou et al. [13] and semi-rigid connection by Fu et al. [23]. Furthermore, in this test, the girder flange fracture caused a sudden drop of the vertical resistance, and the composite floor system could not generate a higher resistance after that. This flange fracture induced the concrete crushing and steel deck tearing around the removed column, which limited the further development of the collapse resistance. In the actual condition, the sudden drop of the vertical resistance might increase the instability in the structure. Hence, it would be helpful to delay the flange fracture of the rigid girder-to-column connection in the penultimate edge column removal scenario. The improved rigid connection proposed by Qin et al. [26] would be a good choice to improve the collapse resistance of the floor system. Fig. 24 shows the configuration of this improved rigid connection, in which, the cover plates can postpone the flange fracture.

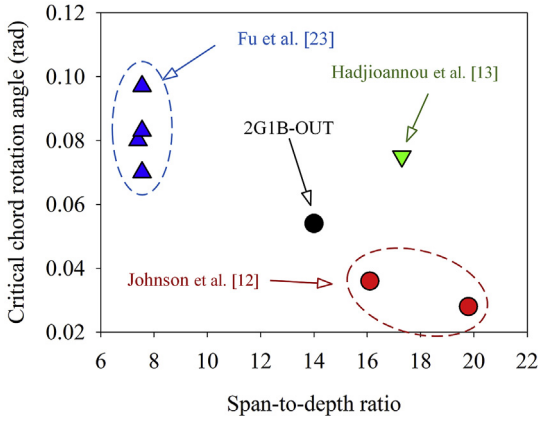

Fig. 23. The critical chord rotation angle in different composite floor tests.

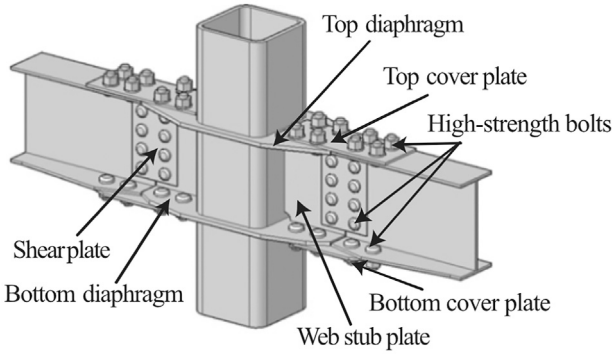

Fig. 24. Configuration of the improved rigid connection proposed by Qin et al. [26].

The load-carrying capacities are also compared in Table 4. Considering the span length and span-to-depth ratio, the specimen in this study was more comparable with those conducted by Johnson et al. [12] and Hadjioannou et al. [13], but the load-carrying capacity of this specimen was much higher. This was partly caused by the relatively larger girder section used in this specimen, which was similar to the girder section used in EC-G [12], but larger than the perimeter beam sections used in EC-B [12] and ECL [13]. Nevertheless, the enhancement in the load-carrying capacity was also attributed to the girder-to-column moment connection. As the girder section used in 2G1B-OUT was similar with the girder used in EC-G [12], but the load-carrying capacity of 2GB-OUT (29.5 kN/m^2) was much higher than the 4.0 kN/ m^2 in EC-G. The numerical simulation conducted by Main and Liu [27] also confirmed that the frame with moment connection was more robust than the same frame with simple connection. Moreover, continuous arrangement and relatively larger thickness of the steel deck in 2G1B-OUT also

contributed to the floor's capacity. Compared with the load combination 1.2DL + 0.5LL, the load-carrying capacities of the floor systems tested by Johnson et al. [12], Hadjioannou et al. [13], and Fu et al. [23] were about 0.6, 1.7, 8.1–15.3 times the load combination, while the floor system in this study could sustain about 4.1 times the load combination. The load-carrying capacities in Fu et al. [23] were much higher than others, which were benefited much from the smaller span-to-depth ratio, smaller span length, relatively larger girder section, and enhanced slab strength. Furthermore, re-entrant steel deck was used in Fu et al. [23], which usually stronger than the composite slab with trapezoidal steel deck [28], as the interlocking action resulted from inverted triangle bulges in the re-entrant steel deck was absent in the trapezoidal composite slabs.

5. Conclusions

In this paper, a 2 × 1 bay full-scale composite floor system was properly designed and quasi-statically pushed down to failure under a penultimate edge column removal scenario. The load-displacement response curve was obtained, and the resisting mechanisms were discussed. The contribution of the respective mechanism in the floor system was quantified separately, and the load redistribution among the columns was also measured. Following conclusions are drawn from this study:

(1) The maximum static or dynamic load carrying capacity of the tested specimen is 4.2 times or 3.6 times of the ASCE load combination for accidental events (1.2 DL + 0.5 LL), indicating this typical steel-concrete composite floor system commonly used in East Asia can prevent the progressive collapse led by the edge column loss.
(2) The maximum resistance is achieved at the flexural stage, being only slightly (6.3%) higher than the predicted value using the yield-line method, which implies the flexural resistance is the main resistant mechanism. After the complete failure of the girder-to-column connection, the experimentally measured load is 15.9% ~ 24.5% higher than the yield line prediction due to neglecting the contribution of the slab tensile membrane action.
(3) Compared with experimental results from the previous composite floor tests, the girder-to-column moment connection and the continuous steel deck employed in this study could improve the load-carrying capacity of the composite floor system. However, in this study, the girder flange connected to the removed column fractured at a relatively small chord rotation angle. This flange fracture induced the concrete crushing and steel deck tearing around the removed column, which limited the further development of the collapse resistance. Therefore, an enhanced girder-to-column moment connection that could delay the flange fracture would benefit the progressive collapse resistance of the composite floor system.

Acknowledgments

The research presented in this paper was sponsored by the State Key Laboratory of Diaster Reduction in Civil Engineering (Tongji University) through Grant Nos. SLDRCE19-A-03 and Natural Science Foundation of China (NSFC) through Grant No. 51378380. Any opinions, findings, conclusions, and recommendations expressed in this paper are those of the authors and do not necessarily reflect the views of the sponsors.

References

[1] U. Starossek, Progressive Collapse of Structures, Thomas Telford, London, U. K, 2009.
[2] GSA, General Services Administration, Alternate Path Analysis & Design Guidelines for Progressive Collapse Resistance (Washington, DC), 2013.
[3] DoD, Department of Defense. Design of buildings to resist progressive collapse, Unified Facilities Criteria UFC 4-023-03 (Washington, DC), 2016.
[4] H. Li, X. Cai, L. Zhang, B. Zhang, W. Wang, Progressive collapse of steel moment-resisting frame subjected to loss of interior column: experimental tests, Eng. Struct. 150 (2017) 203–220.
[5] S.T. Hoffman, L.A. Fahnestock, Behavior of multi-story steel buildings under dynamic column loss scenarios, Steel Compos. Struct. 11 (2) (2011) 149–168.
[6] F. Sadek, S. El-Tawil, H.S. Lew, Robustness of composite floor systems with shear connections: Modeling, simulation, and evaluation, J. Struct. Eng. 134 (11) (2008) 1717–1725.
[7] Y. Alashker, H. Li, S. El-Tawil, Approximations in progressive collapse modeling, J. Struct. Eng. 137 (9) (2011) 914–924.
[8] Y. Alashker, S. El-Tawil, F. Sadek, Progressive collapse resistance of steel-concrete composite floors, J. Struct. Eng. 136 (10) (2010) 1187–1196.
[9] Y. Alashker, S. El-Tawil, A design-oriented model for the collapse resistance of composite floors subjected to column loss, J. Constr. Steel Res. 67 (1) (2011) 84–92.
[10] Li H. Modeling, Behavior and Design of Collapse-Resistant Steel Frame Buildings (PhD Thesis), University of Michigan, Ann Arbor, MI, 2013.
[11] J.A. Main, J. Liu, Robustness of prototype steel frame buildings against column loss: assessment and comparisons, Struct. Cong. (2013) 43–54.
[12] E.S. Johnson, J.E. Meissner, L.A. Fahnestock, Experimental behavior of a half-scale steel concrete composite floor system subjected to column removal scenarios, J. Struct. Eng. 142 (2) (2015), 04015133.
[13] M. Hadjioannou, S. Donahue, E.B. Williamson, et al., Large-scale experimental tests of composite steel floor systems subjected to column loss scenarios, J. Struct. Eng. 144 (2) (2017), 04017184.
[14] Q.N. Fu, K.H. Tan, X.H. Zhou, et al., Load-resisting mechanisms of 3D composite floor systems under internal column-removal scenario, Eng. Struct. 148 (2017) 357–372.
[15] H.G. Harris, Sabnis G. Structural Modeling and Experimental Techniques, CRC Press, 1999.
[16] D. Mitchell, W.D. Cook, Preventing progressive collapse of slab structures, J. Struct. Eng. 110 (7) (1984) 1513–1532.
[17] Ministry of Housing and Urban-Rural Development of the People's Republic of China, Code for Design of Steel Structure. GB50017-2003, 2003.
[18] Ministry of Housing and Urban-Rural Development of the People's Republic of China, Code for Seismic Design of Buildings. GB50011–2010, 2010.
[19] ASCE 7-16, Minimum Design Loads and Associated Criteria for Buildings and Other Structures, American Society of Civil Engineers, Reston, Virginia, 2017.
[20] B.A. Izzuddin, A.G. Vlassis, A.Y. Elghazouli, et al., Progressive collapse of multi-storey buildings due to sudden column loss—part I: simplified assessment framework, Eng. Struct. 30 (5) (2008) 1308–1318.
[21] P.X. Dat, K.H. Tan, Experimental response of beam-slab substructures subject to penultimate-external column removal, J. Struct. Eng. 141 (7) (2014), 04014170.
[22] R.P. Johnson, Composite Structures of Steel and Concrete: Beams, Slabs, Columns and Frames for Buildings, John Wiley & Sons, 2004.
[23] Q.N. Fu, K.H. Tan, X.H. Zhou, et al., Three-dimensional composite floor systems under column-removal scenarios, J. Struct. Eng. 144 (10) (2018), 04018196.
[24] T. Francisco, J. Liu, Experimental characterization of a composite slab subjected to simulated column removal loading, J. Struct. Eng. 142 (1) (2015), 04015090.
[25] C.H. Lee, S. Kim, K.H. Han, et al., Simplified nonlinear progressive collapse analysis of welded steel moment frames, J. Constr. Steel Res. 65 (5) (2009) 1130–1137.
[26] X. Qin, W. Wang, Y. Chen, et al., Experimental study of through diaphragm connection types under a column removal scenario, J. Constr. Steel Res. 112 (2015) 293–304.
[27] J.A. Main, J. Liu, Robustness of Prototype Steel Frame Buildings against Column Loss: Assessment and Comparisons//Structures Congress 2013: Bridging your Passion with your Profession, 2013, pp. 43–54.
[28] J. Wang, W. Wang, D.E. Lehman, et al., Effects of different steel-concrete composite slabs on rigid steel beam-column connection under a column removal scenario, J. Constr. Steel Res. 153 (2019) 55–70.